Journal of Polymers and the Environment (2020) 28:1492–1502
https://doi.org/10.1007/s10924-020-01702-1

ORIGINAL PAPER

Efficient Removal of Dyes from Aqueous Solution by a Porous Sodium Alginate/gelatin/graphene Oxide Triple-network Composite Aerogel

Chenlu Jiao[1] · Tingting Li[1] · Jian Wang[1] · Hao Wang[1] · Xiaoli Zhang[1] · Xiaojian Han[1] · Zhaofang Du[1] · Yali Shang[1] · Yuyue Chen[2]

Published online: 18 March 2020

Abstract
A three-dimensional (3D) robust sodium alginate/gelatin/graphene oxide (SGGO) triple-network composite aerogel was designed using a "hydrophilic assembly–sustained release gelation" two-step method. The resulting SGGO aerogel has an ordered fishing net-like microstructure, low density (16.2 mg/cm^3), high porosity (93.5%), and abundant functional groups when only 3 wt% GO was incorporated. The reinforced mechanical strength can reach 0.37 MPa and 0.12 MPa under dry and wet states, respectively, and the dry strength can still reach 0.31 MPa without a significant loss after five compression cycles. A batch adsorption experiment was performed as a function of pH, contact time and initial concentration. Adsorption behavior followed the pseudo second-order kinetic model and Langmuir isotherm, yielding the maximum monolayer adsorption capacity of 322.6 mg/g and 196.8 mg/g for Methylene blue (MB) and Congo red (CR), respectively. Moreover, thermodynamic studies indicated a spontaneous and endothermic adsorption process. After five regeneration cycles, the adsorption capacity can reach 88.4% and 86.5% of the initial values for MB and CR, demonstrating a high-performance, recyclable and promising candidate for dye wastewater treatment.

Keywords Sodium alginate · Gelatin · Graphene oxide · Aerogel · Dye removal

Introduction

Dye wastewater generated from various industries, including printing and dyeing, synthesis, leather, electroplating, and cosmetic, has received considerable attention owing to its deep chromaticity, high toxicity, and teratogenicity [1, 2]. Additionally, most of the dye-containing effluents are stable and nondegradable in the natural environment. Therefore, removal of dyes from industrial effluents is essential for the protection of water sources [3]. Many strategies and new technologies spinning from chemical precipitation [4], coagulation/flocculation [5], electrodialysis [6], photocatalytic degradation [7] to adsorption [8] have been developed to treat dye wastewater. Among these methods, adsorption is proved to be a more competitive technology owing to its simplicity, high efficiency, low cost, wide-ranging availability, and eco-friendliness [9].

Aerogels, typical three-dimensional (3D) porous materials, are known as one of the most attractive adsorbents because of their low density, high porosity, large specific surface area, high adsorption capacity, and self-supporting configuration [10, 11]. In the specific field of wastewater treatment, biomass-based aerogels, have attracted much attention as natural and sustainable materials [12]. Sodium alginate (SA), an abundant, renewable, and environment-friendly natural polysaccharide, is composed of (1→4)-linked block polymers of α-L-guluronic acid and β-D-mannuronic acid or their copolymers in varying proportions [13, 14]. Offering merits such as abundance, hydrophilicity, biocompatibility, gel-forming ability, and biodegradability combined with the ability to form stable hydrogel due to the presence of specially coordinated carboxylic binding sites, SA aerogels have been used for dye removal from effluents [15, 16]. Even so, large-scale utilization of pure SA aerogels for dye wastewater treatment is still limited due to some unsatisfactory structural properties such as weak mechanical strength, structural

✉ Chenlu Jiao
jiaochenlu@ahau.edu.cn; jiaochenlu2013@163.com

[1] College of Light-Textile Engineering and Art, Anhui Agricultural University, Hefei 230036, Anhui, China

[2] College of Textile and Clothing Engineering, Soochow University, Suzhou 215123, Jiangsu, China

nonuniformity, and fragile collapse [17, 18]. To improve the structure and performance of SA aerogels, three commonly strategies are used to achieve complementary functional advantages: (1) blending of two or more polymers to construct double or multiple networks [19–22]; (2) doping of organic or inorganic nanoparticle fillers to reinforce and toughen gel networks [21, 23, 24]; (3) assemble of high-strength materials in mesoscopic scale [25].

Gelatin (Gel) is a partial derivative of collagen with abundant hydroxyl, carboxyl, and amino groups in its molecule chains, offering easy gelation and functionalization [26]. Gel has distinct advantages including low cost, water solubility, biocompatibility, biodegradability, and remarkable affinity to proteins; therefore, it has been set as a starting material to build 3D structures [27, 28]. Herein, owing to the good compatibility of SA and Gel, a cross-linked double network will be formed by electrostatic interaction and hydrogen bond [28, 29]. Among this specific networks, Gel molecule chains also work as blockers, decreasing the possibility of direct contact between the G units of SA chains and Ca^{2+} ions in the following gelation process and providing more time and space to form a homogeneous double network.

The effect of double network on aerogel's strength enhancement is limited, and a more direct and effective approach is to dope rigid reinforcing (nano) fillers. Graphene oxide (GO), for example, a two-dimensional (2D) carbonic material with excellent mechanical property, high specific surface area, and rich oxygen-containing functional groups, makes GO compatible with water-soluble polymer matrices. Recently, many studies have reported the reinforcement function of GO, rendering it to be an ideal reinforcing filler for composite monoliths [17, 30, 31].

In the past few years, many synthetic processes have been developed for SA/GO composites, as well as their applications in drug delivery systems [32, 33], triboelectric generators [34], and wastewater remediation [35–37]. However, it is still difficult to obtain aerogels with stable structures and good performances by these methods. In this study, a combined technology of multiple network and filler reinforcement was used. A mechanically strong and recyclable SA/Gel/GO triple-network monolithic aerogel was fabricated via a "hydrophilic assembly–sustained release gelation" two-step method. Herein, SA and Gel were selected as 3D scaffold materials, and GO nanosheets acted as a reinforcing filler and also like a "crosslinker" to connect and strengthen the compound network. The assembly mechanism as well as the effects of GO nanosheet content on the mechanical strength and adsorption capacity of dyes from aqueous solution is presented. Overall, this study provides new insights into engineering reliable biomass-based aerogel adsorbents for wastewater treatment.

Materials and Methods

Materials

Sodium alginate (SA, medium viscosity, M = 250,000 g/mol) and gelatin (Gel) were obtained from Aladdin Industrial Co., Ltd (Shanghai, China). Graphene oxide (GO) synthesized from natural graphite power (99.95%, Aladdin Reagent) using a modified Hummer's method was dispersed in deionized water [38]. Hydrochloric acid (HCl), sodium hydroxide (NaOH), calcium carbonate ($CaCO_3$), D-glucono-δ-lactone (GDL), Methylene blue (MB), and Congo red (CR) were purchased from Sinopharm Chemical Reagent Co., Ltd. (Hefei, China).

Preparation of SGGO Aerogel

In a typical synthesis, solutions of SA and Gel, 2 wt%, were prepared using deionized water at 50 °C. Solutions of 50 mL SA and 50 mL Gel were mixed together to obtain a mixture at room temperature. Then, a suspension with 60 mg GO was added, and the mixture was ultrasonicated for 30 min to obtain a homogeneous SA/Gel/GO (SGGO) hybrid sol. Subsequently, a predetermined amount of $CaCO_3$ was directly added into the sol and homogenized using Ultraturrax (IKA, Germany), followed by adding freshly prepared 1 mol/L GDL aqueous solution. Here, the molar ratio of $CaCO_3$ to GDL is about 1:2 to maintain an approximately neutral condition [12, 39]. The hybrid sol was casted into molds, forming a homogeneous hydrogel in 30 min. Then, monolithic SGGO aerogels with 3 wt% GO content was obtained after a freeze-drying treatment (abbreviated as SGGO-3). For comparasion, SA/Gel aerogels without GO and SGGO aerogels with various GO contents were synthesized following the same procedure.

Characterization

The morphology of GO was analysed by atomic force microscopy (AFM, Dimension Icon, Bruker, Germany). A field-emission scanning electron microscope (FE-SEM, S-4800, Hitachi, Japan) was used to observe the microstructure and morphology of aerogels. The FTIR spectra of SA, Gel, GO, and SGGO aerogel were recorded using a Fourier transform infrared spectrometer (FTIR, Nicolet 5700, Thermo Nicolet, USA). The compressive strength was measured using a universal testing machine (Instron-3365, Instron, USA) until the strain reached 60%.

Porosity of Aerogel

The porosity of SGGO aerogels was calculated based on the following equation:

$$\text{Porosity}(\%) = \frac{Vt - Va}{Vt} \times 100 = \frac{Vt - Wt/\rho}{Vt} \times 100 \quad (1)$$

where V_t (cm^3) and V_a (cm^3) are the total volume and actual volume of aerogel, respectively. W_t (g) is the weight of aerogel, and ρ (g/cm^3) denotes the density of aerogel. Each sample was measured in triplicate, and the average value was calculated.

Adsorption and Desorption Experiments

Typically, 0.1 g SGGO aerogel was placed into a 250 mL conical flask containing 100 mL of dye solution at 298 K. The initial concentration was 500 mg/L if not specified. The initial pH values of solutions were adjusted using dilute HCl or NaOH solution, and the solutions were shaken at room temperature. At the end of preset time intervals, the residual dye concentration in supernatant was measured by a UV–vis spectrophotometer (U-3010, Hitachi, Japan). The adsorption capacity Q_t (mg/g) was calculated according to the following equation:

$$Qt = \frac{(Co - Ct)V}{m} \quad (2)$$

where C_o (mg/L) is the initial concentration of dye solution; Q_t (mg/g) and C_t (mg/L) represent the adsorption capacity and dye concentration at a given time, respectively. V (L) denotes the volume of dye solution, and m (g) is the mass of SGGO aerogel.

After adsorption, the used SGGO aerogel was immersed in 0.07 M NaOH or HCl solution, and the solution was stirred for 1 h. Then, the SGGO aerogel was separated and washed with abundant deionized water to remove the residual eluent to obtain the aerogel ready for the next adsorption test.

Results and Discussion

Characterization of GO

Figure 1a shows the photograph of GO suspension used to construct the SGGO aerogels. The exfoliated GO readily dispersed in deionized water with mild ultrasonic treatment and formed a transparent suspension that can be maintained for several months. The AFM photograph of GO nanosheets shows that they have one or several layers with each thickness of ca. 1 nm (Fig. 1b). This well dispersed GO suspension is useful for the construction of porous SGGO aerogels.

Assembly Mechanism of SGGO Aerogel

It is challenging to fabricate versatile composite aerogels due to difficulty in coordinating the structures and properties to satisfy different demands. Herein, an efficient "hydrophilic assembly–sustained release gelation" two-step method and possible assembly mechanism are proposed in Fig. 2. First, SA and Gel chains acted as 3D scaffold materials to form a compound network. When embedding GO, owing to the amphipathicity of GO nanosheets, an effective "hydrophilic assembly" might occur, driven by the hydrophilic edges (oxygen-containing groups) of GO nanosheets and active sites of compound network structure via electrostatic interaction and hydrogen bond, thus generating an intercalated structure as shown in Fig. 2c [40]. Then, the "sustained release gelation" strategy was used to obtain a homogeneous and ordered structure, by the *in-situ* release of Ca^{2+} ions from $CaCO_3$ induced by the hydrolysis of GDL to reduce the pH value, forming a typical calcium-alginate "egg-box" model (Fig. 2e). Hence, in the assembly process, GO nanosheets worked as a reinforcing filler and also like a "crosslinker" to connect the double networks and construct a uniform and robust SGGO aerogel. Furthermore, GO nanosheets with abundant active groups have the potential

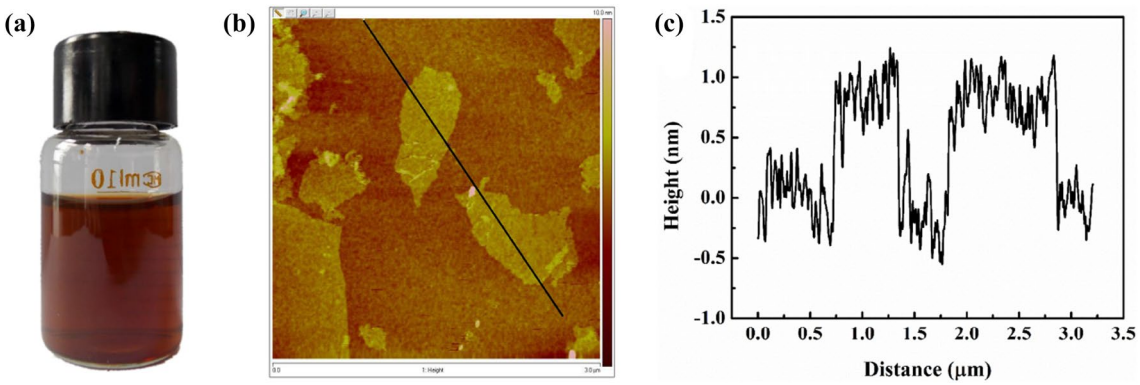

Fig. 1 Photograph of GO suspension (**a**), AFM image (**b**) and height profile (**c**) of GO nanosheets

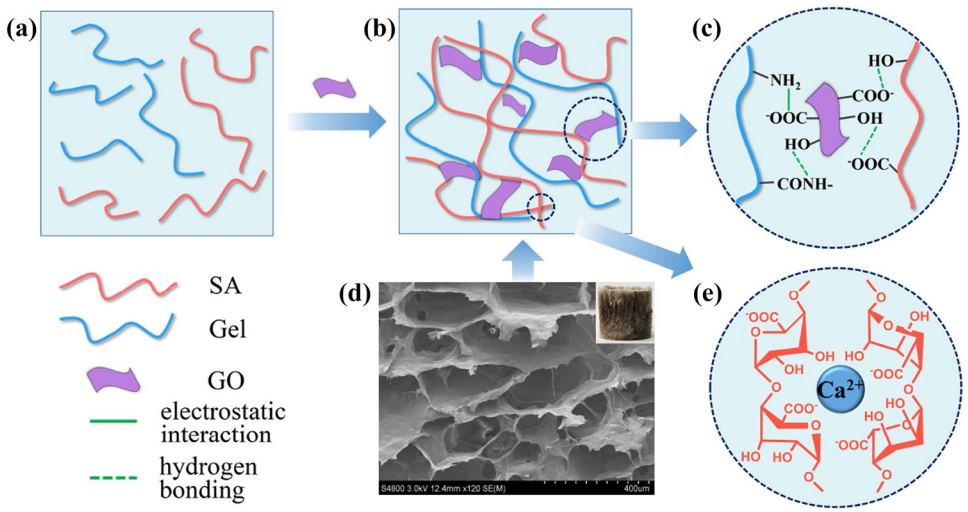

Fig. 2 Schematic depiction of fabrication process and possible assembly mechanism of SGGO aerogel

to improve the adsorption capacity of composite aerogels. The double networks can simultaneously prevent the GO nanosheets from stacking and enhance the connectivity of cell walls, thus promoting the formation of a uniform and ordered structure (Fig. 2d).

Structure Characterization of SGGO Aerogel

As shown in Fig. 3, all aerogels display a porous structure, which is crucial to facilitate dye adsorption. Apparently, the SA/Gel aerogel has a 3D framework with a randomly interconnected macroporous structure (Fig. 3a). While for SGGO aerogels (Fig. 3b–e), the pores became more regular and denser with increasing GO content, exhibiting a fishing net-like porous structure with pores in the range of tens to hundreds of microns. This is probably because the crosslinking of GO nanosheets to pore wall will divide a large pore into several small pores and support the shape and prevent the contraction of pores (Fig. 2b). Moreover, compared with a smooth cell wall structure of SA/Gel aerogel in further magnified image of Fig. 3a, Fig. 3f shows an undulating wrinkled lamellar structure of SGGO-4 aerogel, typical morphology of GO nanosheets. Also, slight agglomeration and cluster formation are observed in the GO nanosheets in the SGGO

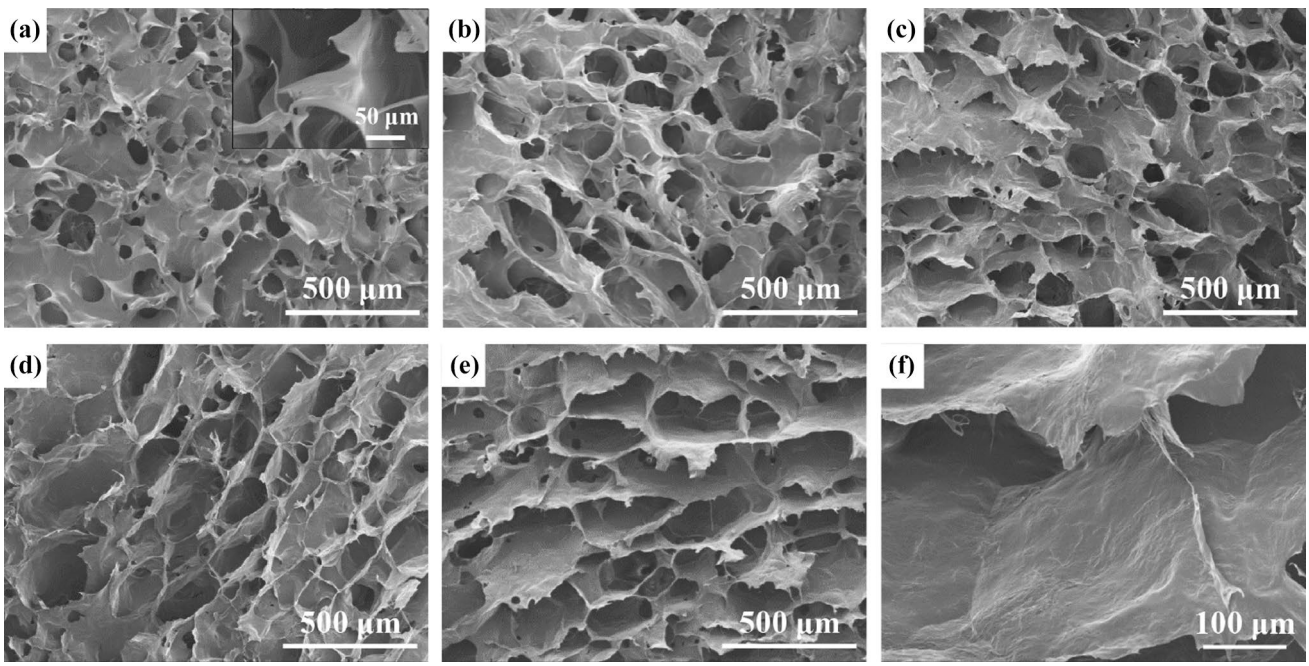

Fig. 3 SEM images of SA/Gel aerogel (**a**) and SGGO aerogels with various GO contents: SGGO-1 (**b**), SGGO-2 (**c**), SGGO-3 (**d**), SGGO-4 (**e**), and further magnification of SGGO-4 aerogel (**f**)

aerogels, due to the interaction between GO nanosheets and the active chains of SA and Gel in the assembly process, subsequently forming a homogeneous and reinforced triple-network structure and increasing the specific surface area. The results indicate that GO nanosheets are beneficial for improving the adsorption capacity.

The SGGO aerogels are lightweight and full of pores. Figure 4 shows the trend of porosity and density with the addition of GO nanosheets. The density of aerogels shows almost a linear increase with respect to the concentration of GO, while the porosity does not depend on the GO content and is in the range of 93–93.5%. This is probably because the GO concentration might be too low to have a measurable effect. Overall, all the porous SGGO aerogels have a high porosity (over 93%) that desirably facilitates dye removal.

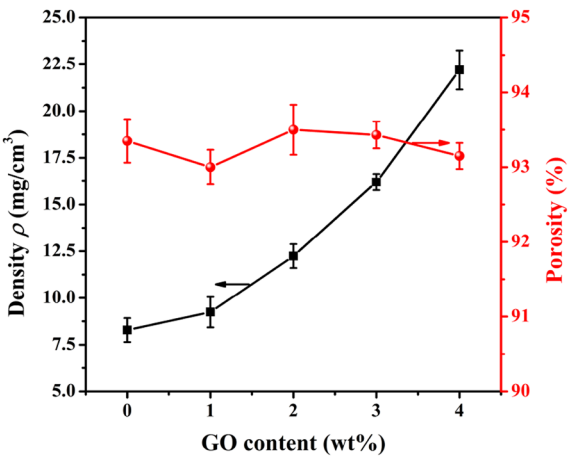

Fig. 4 Bulk density and porosity of SGGO aerogels with different GO contents

FTIR Analysis of SGGO Aerogel

To further analyze the interactions between the components, changes to the chemical structure of SA, Gel, and GO were investigated, as shown in Fig. 5. The spectra of SA and Gel were recorded as the control. The band of SA (curve a) at 1616 cm^{-1} represents the asymmetric stretching vibration of $-COO^-$ [41]. In the spectrum of Gel (curve b), the peaks at 1655 cm^{-1} and 1539 cm^{-1} can be attributed to C=O stretching vibration (amide I) and N–H bending vibration (amide II) [42]. The characteristic peaks at 1732 cm^{-1} and 1622 cm^{-1} for GO (curve c) correspond to the stretching vibrations of –COOH and C=C groups in the sp^2 carbon skeletal network, respectively [17, 43]. For SGGO aerogel (curve d), the 2931 cm^{-1} band of C–H asymmetric stretching vibration is slightly slow, owing to the limited C-H stretching by "egg-box" model formed via SA macromolecules and Ca^{2+} ions [30]. Moreover, the downshifted peaks at 3379 cm^{-1}, 1615 cm^{-1}, and 1532 cm^{-1} of SGGO aerogel

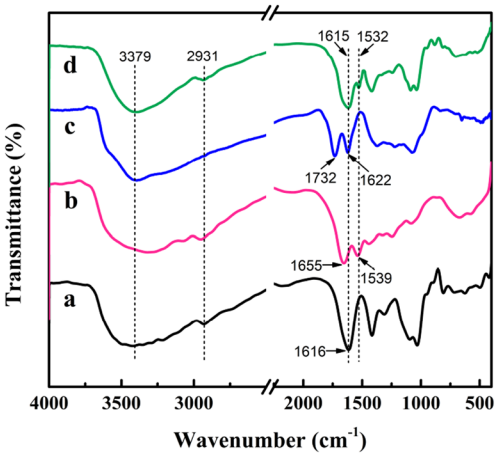

Fig. 5 FTIR spectra of SA (a), Gel (b), GO (c), and SGGO composite aerogel (d)

suggest the presence of hydrogen bond [40], which shows the interaction between GO nanosheets and SA/Gel chains and is consistent with the assembly mechanism shown in Fig. 2c.

Mechanical Property of SGGO Aerogel

A successful adsorbent should have high mechanical property for supporting the configuration and regeneration ability. Figure 6 reveals the effect of GO concentration on the compressive strength of porous SGGO monoliths. As shown in Fig. 6a, the compressive strength of the SGGO aerogels clearly increased with increasing GO content, and the dry and wet strength reached 0.37 MPa and 0.12 MPa at 3 wt% GO content, followed by no apparent improvement with further increase in GO content. Two distinct stages were observed from the stress–strain curves in Fig. 6a, an initial linear region at the strain < 30% and a densification region at the strain > 30%, suggesting the nature of porous structures [44]. In the first stage, owing to the high porosity and flexibility, air escaped from interspace. As the pressure was further increased, all the lamellas of organized SGGO aerogels were compressed to support the load, thus generating a greater compression strength.

The compression diagrams of SA/Gel and SGGO aerogels are shown in Figs. 6c and 6d. The improvement in mechanical strength can be attributed to the network structure of aerogels. Oxygen-containing groups of GO nanosheets can well interact with SA and Gel chains through "hydrophilic assembly" and then provide effective load transfer between the SA/Gel network matrix and GO nanosheets. Hence, the SGGO aerogel can support a larger load compared to SA/Gel aerogel. Additionally, Fig. 6b displays the cyclic compressive property of SGGO-3 aerogel. After five compression cycles, the dry strength can be still maintained at 0.31 MPa

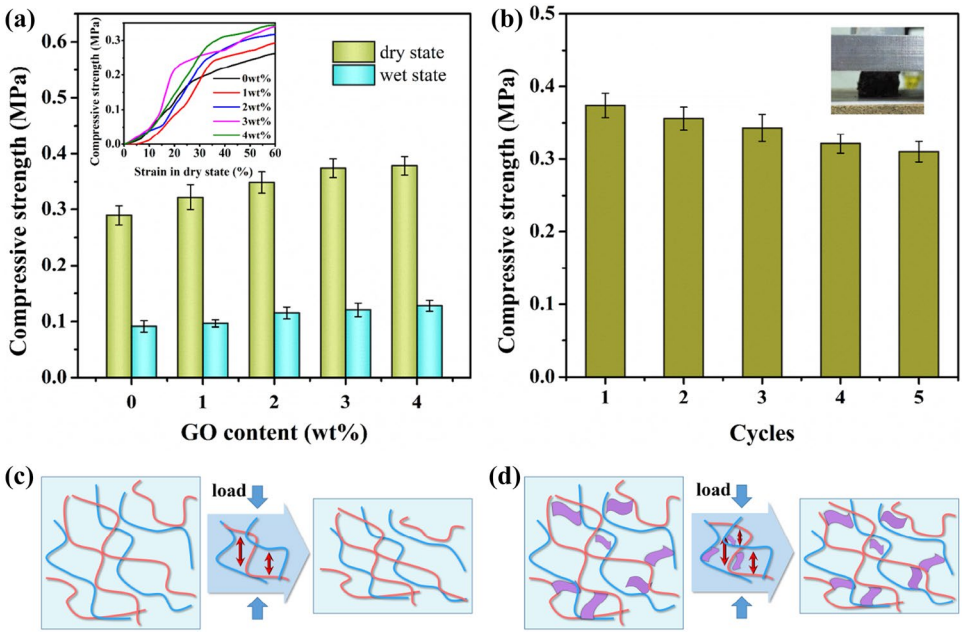

Fig. 6 Compressive strength of SGGO aerogels with various GO contents in dry and wet states (**a**), SGGO-3 aerogel for different cycles in dry state (**b**), and possible compressive mechanism of SA/Gel aerogel (**c**) and SGGO aerogel (**d**)

without significant loss, significantly higher than similar reports [45–47], thus indicating a mechanically strong aerogel with excellent structure stability.

Effect of pH and GO Content on Dye Adsorption

The solution pH is a considerable factor in a sorption study, which can vary the surface charge of adsorbents and dyes. As shown in Fig. 7a, the pH range of 4–10 was set, because concentrated acidic and alkaline environments can influence the conjugated structures of dye molecules [28, 48]. The equalized adsorption capacity Q_e of MB increased with increasing pH. In the acid solution, the SGGO aerogel was protonated, leading to a lower Q_e because excessive H^+ ions on the surface of SGGO aerogel compete with the MB molecules. In the alkaline solution, the amount of adsorption rapidly increased on account of the electrostatic attraction between deprotonated aerogel and cationic MB molecules. For CR dye, the Q_e first increased as the pH increased from 4 to 6 and then gradually decreased with further increase in pH to 10. In fact, CR has a p*K*a of 4.5–5.5, and it would be protonated because of the nitrogen atoms and sulfonate groups present in the acid solution [49], leading to electrostatic repulsion between the protonated SGGO aerogel and cationic CR molecules. In the alkaline condition, the electrostatic repulsion between deprotonated SGGO aerogel and anionic CR molecules still hindered the adsorption behavior. Therefore, the adsorption of dyes was significantly affected by the change in pH, and the electrostatic interaction played an important role in the adsorption performance. Therefore, the adsorption amounts of MB and

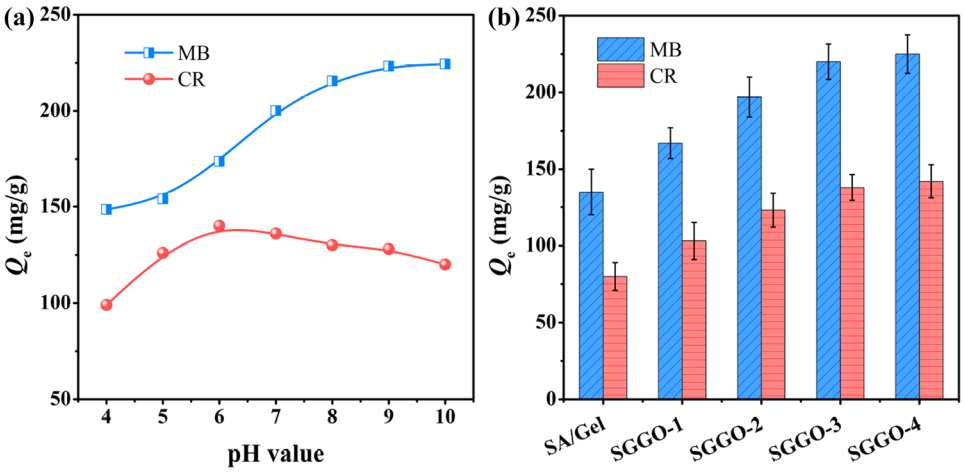

Fig. 7 (**a**) The effect of initial pH value on the adsorption of MB and CR on SGGO-3 aerogel, and (**b**) adsorption capacities of aerogels with various GO contents towards MB and CR

CR of SGGO aerogels were measured at optimal pH values in the following experiment.

As shown in Fig. 7b, the Q_e values of SGGO aerogels with various GO contents for dyes were investigated. The SA/Gel aerogel showed a relatively low Q_e towards MB and CR. After loading GO, the value of Q_e obviously increased for both MB and CR, and no significant change was observed after 3 wt% GO was incorporated. Therefore, SGGO-3 aerogel was selected for the following study because both adsorption capacity and mechanical strength reached the optimal values. The incorporation of GO enhanced the surface area of SGGO aerogels and endowed more functional groups, which further improved the adsorption capacity of SGGO aerogels. Furthermore, MB showed better adsorption capacity compared to CR. This can be explained by the electrostatic force, i.e. the surface of SGGO aerogel loaded with more negative charges is advantgeous for the adsorption of positively charged MB molecules.

Adsorption Kinetics

Adsorption kinetic study is an essential way to analyze the adsorption mechanism and control the residual time of adsorption process, which can provide valuable experimental parameters for determining practical applications. The adsorption behaviors of SGGO-3 aerogels for MB and CR are shown in Fig. 8a. The adsorption was rapid in the first 60 min, and no significant change was observed after 90 min and 120 min for MB and CR, respectively.

To better understand the adsorption behaviors, the pseudo first-order model and pseudo second-order model were employed to analyze the results, as shown in Eqs. (3) and (4) [50, 51],

$$\ln(Q1\mathrm{e} - Q\mathrm{t}) = \ln Q1e - k1t \tag{3}$$

$$\frac{t}{Q\mathrm{t}} = \frac{t}{Q2e} + \frac{1}{k2Q2e^2} \tag{4}$$

where Q_{1e} (mg/g) and Q_{2e} (mg/g) are the equalized adsorption capacities estimated from the pseudo first-order and pseudo second-order model equations, respectively. k_1 (min^{-1}) and k_2 (g/mg min) represent the rate constants calculated from the slopes/intercepts of the fitting equations (Figs. 8b and 8c).

All the corresponding parameters and experimental adsorption capacities are listed in Table 1. The adsorption of MB and CR followed the pseudo second-order model, with both R^2 values greater than 0.99. Moreover, the theoretical adsorption capacities (Q_{2e}) calculated from the pseudo-second-order kinetic equation are 241.5 and 152.7 mg/g for MB and CR, respectively, consistent with the experimental values. This indicates that the pseudo-second-order model can describe the adsorption process more reasonably.

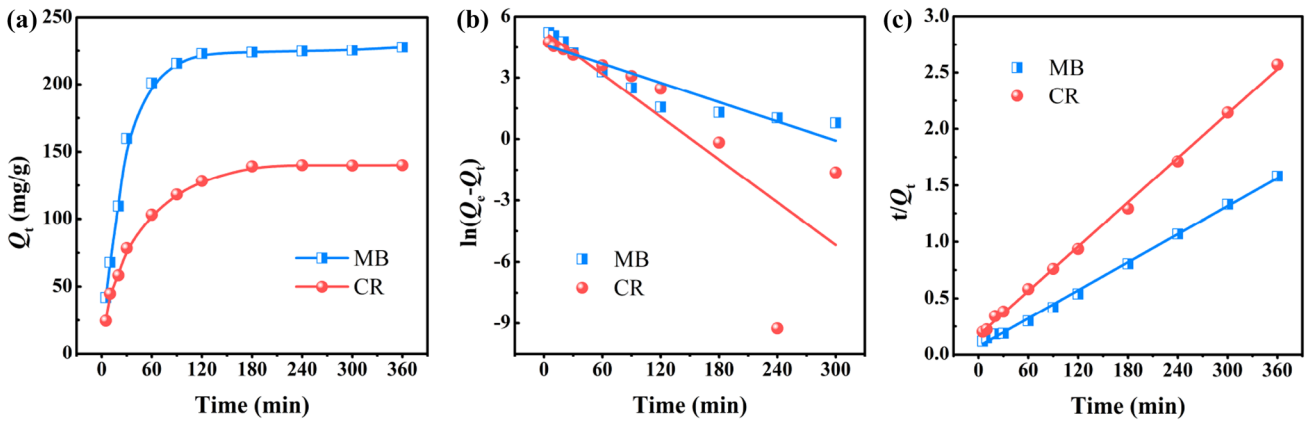

Fig. 8 (**a**) Adsorption behaviors of SGGO-3 aerogels for MB and CR. (**b**) The linear plots of pseudo-first-order kinetic model, and (**c**) pseudo-second-order kinetic model

Table 1 Kinetic parameters of the pseudo-first-order and pseudo-second-order models for MB and CR on SGGO-3 aerogel

Adsorbates	Q_{exp} (mg g^{-1})	Pseudo-first-order model			Pseudo-second-order model		
		$Q_{1e,cal}$ (mg g^{-1})	k_1 (min^{-1})	R^2	$Q_{2e,cal}$ (mg g^{-1})	$k_2\times10^4$ (g mg^{-1} min^{-1})	R^2
MB	227.7	102.8	0.0157	0.8324	241.5	2.3096	0.9977
CR	140.1	193.9	0.0348	0.6418	152.7	2.4996	0.9985

Adsorption Isotherm

As shown in Fig. 9a, the adsorption isotherms of both MB and CR have the same qualitative trend: The Q_e first increases rapidly under low dye concentrations and then gradually reaches a plateau that is distinctive of an equilibrium saturation point, indicating a typical homogeneous adsorption process. This can be explained by the increasing driving force produced by the concentration gradient, which intensifies the interaction between SGGO aerogel and dye molecules to some extent [52, 53].

To describe the interactive behavior between dyes and SGGO aerogel, two classical adsorption isotherm models, namely, Langmuir and Freundlich isotherms, were analyzed to evaluate the adsorption process [54]. Assuming that the adsorption occurs at specific homogeneous sites of SGGO aerogel with a monolayer coverage of dyes, the Langmuir isotherm can be expressed as follows:

$$\frac{Ce}{Qe} = \frac{Ce}{Q\max} + \frac{1}{kLQ\max} \tag{5}$$

where C_e (mg/L) and Q_e (mg/g) are the equilibrium concentration and equilibrated adsorption amount, respectively. Q_{max} (mg/g) is the maximum monolayer capacity calculated from the linear Langmuir equation, and k_L (L/mg) is the Langmuir constant representing the energy of adsorption process. Q_{max} and k_L were determined by plotting C_e/Q_e against C_e (Fig. 9b), and all the parameters are listed in Table 2. Also, another essential parameter known as separation factor R_L is defined based on Eq. 6,

$$RL = \frac{1}{1 + kLCo} \tag{6}$$

where R_L indicates the type of the isotherm unfavorable ($R_L > 1$), linear ($R_L = 1$), favorable ($0 < R_L < 1$), or irreversible ($R_L = 0$). As shown in Table 2, all the values are in the range of 0–1, indicating a favorable adsorption.

The Freundlich isotherm, an empirical model, is based on multilayer adsorption on heterogeneous surfaces, and can be expressed by Eq. 7 [55],

$$\ln Qe = \ln kF + \frac{1}{n}\ln Ce \tag{7}$$

where k_F and n represent the Freundlich constant and heterogeneity factor, which are determined by the intercept and slope of linear plots (Fig. 9c).

The estimated isotherm parameters are listed in Table 2, exhibiting that the Langmuir isotherm model has a higher correlation coefficient ($R^2 > 0.99$), suitable Langmuir constant ($k_L > 0$), and feasible separation factor ($0 < R_L < 1$), indicating a favorable adsorption model. Also, the Q_{max} of aerogel is 322.6 mg/g for MB and 196.8 mg/g for CR, occurring in a monolayer and at a fixed number of binding sites.

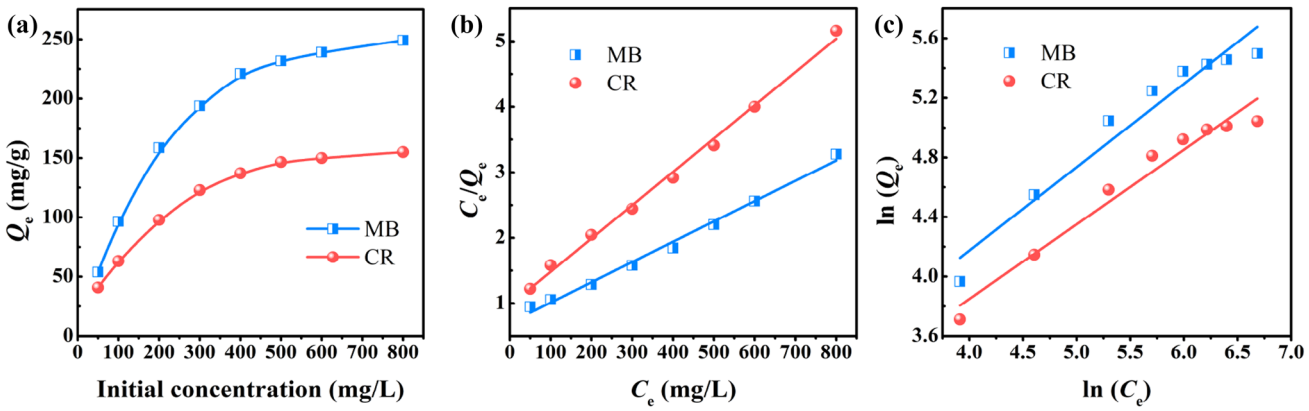

Fig. 9 (**a**) Effect of initial concentration on the absorption capacity of SGGO aerogel for MB and CR. (**b**) Langmuir and (**c**) Freundlich isotherm plots of SGGO aerogel

Table 2 Langmuir and Freundlich parameters for MB and CR on SGGO-3 aerogel

Adsorbates	Langmuir				Freundlich		
	Q_{max} (mg g^{-1})	k_L (L/mg)	R^2	R_L	k_F (L/mg)	n	R^2
MB	322.6	0.0044	0.9909	0.2212–0.8197	6.9291	1.7864	0.9406
CR	196.8	0.0052	0.9951	0.1938–0.7937	6.3280	1.9953	0.9586

Adsorption Thermodynamics

The concept of thermodynamic supposes that in an isolated system where energy cannot be added or lost, the entropy change ($\Delta S°$) is the only driving force [56]. Thermodynamic parameters can estimate the effect of temperature on the adsorption of SGGO-3 aerogel and provide an insight into the adsorption mechanism and behavior. To depict the adsorption process, the enthalpy change ($\Delta H°$), Gibbs free energy change ($\Delta G°$) and $\Delta S°$ can be determined by the Van't Hoff equation [35].

$$\Delta G^0 = -RT\ln(K\mathrm{L}) \tag{8}$$

$$\ln(K\mathrm{L}) = \frac{\Delta S^0}{R} - \frac{\Delta H^0}{RT} \tag{9}$$

where K_L is the Langmuir equilibrium constant (L/mol), R and T are the universal gas constant (8.314 J/mol K) and absolute solution temperature (K), respectively. Take MB as an example, $\Delta H°$ and $\Delta S°$ were calculated from the slope and intercept of the Van't Hoff plot between $\ln(K_L)$ vs. $1/T$, as shown in Fig. 10 [57, 58]. The calculated values at different temperatures are presented in Table 3.

As shown in Table 3, the negative values of $\Delta G°$ for MB reveal the spontaneous nature of adsorption onto SGGO-3 aerogel in the studied ranges of temperature and concentration. Besides, the increasing negative value of $\Delta G°$ at higher temperatures suggests that the adsorption is favorable with increasing temperature. The positive value of $\Delta H°$ confirms the endothermic nature of MB adsorption, indicating that the adsorption capacity of MB increased at a higher temperature. Meanwhile, the positive value of $\Delta S°$ reflects the affinity of SGGO-3 aerogel for MB and the increasing randomness at the solid–liquid interface during the adsorption.

Table 3 Thermodynamic parameters for the adsorption of MB on SGGO-3 aerogel

Temperature (K)	ΔG^0 (kJ/mol)	ΔH^0 (kJ/mol)	ΔS^0 (kJ/mol K)
288	−17.07	8.50	0.09
298	−17.96		
308	−18.79		
318	−19.76		

All the thermodynamic parameters mentioned above suggest that the SGGO aerogel can be used as a highly efficient adsorbent for dye removal from aqueous solutions.

Reusability and Stability Studies

Recyclability is considered an important prerequisite for sustainable and economic applications of adsorbents. As shown in Fig. 11, the SGGO aerogel had good reusable performance with a high adsorption capacity retained. The Qe for MB and CR can be still maintained at 88.4% and 86.5% of their initial values after five sequential adsorption–desorption cycles, demonstrating a benign and sustainable adsorbent.

Conclusions

A 3D robust SGGO triple-network composite aerogel was fabricated using an efficient "hydrophilic assembly–sustained release gelation" two-step method. The micromorphological characterization showed that the SGGO aerogel has a fishing net-like porous structure, and the pores became denser and more regular with the increase in GO content. A

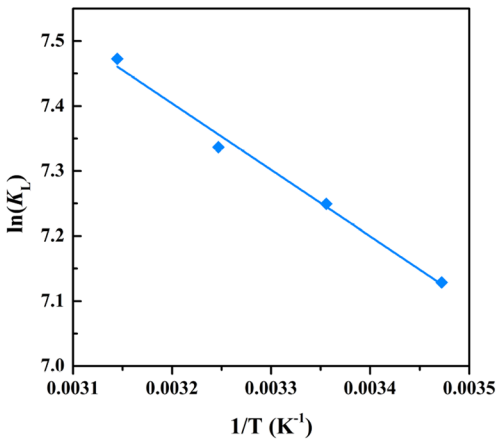

Fig. 10 Regressions of Van't Hoff plot for thermodynamic parameters of MB

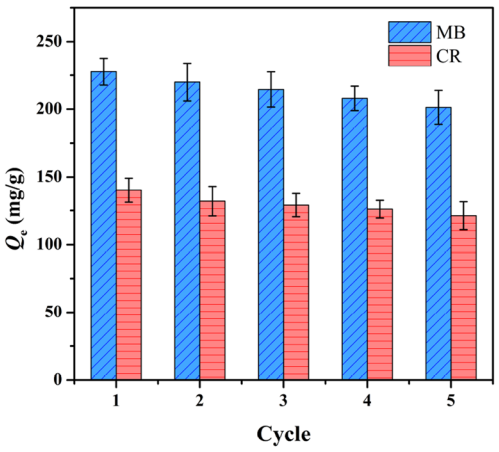

Fig. 11 Cyclic test of the SGGO-3 aerogel for dyes adsorption up to five cycles

strong interaction was observed between the SA/Gel double networks and GO nanosheets. The mechanical strength of SGGO-3 aerogel reached 0.37 MPa and 0.12 MPa under dry and wet states, respectively, obviously superior than similar reports. The adsorption of MB and CR on SGGO aerogel rapidly occurred, mainly through electrostatic interaction. Adsorption behavior obeyed the pseudo second-order kinetic model and Langmuir isotherm, indicating a monolayer adsorption with maximum capacity of 322.6 mg/g and 196.8 mg/g for MB and CR at 298 K, respectively. Thermodynamic analyses indicate that the dye uptake on SGGO aerogel was spontaneous and endothermic. After five regeneration cycles, the SGGO aerogel can maintain 88.4% and 86.5% of their initial adsorption capacities for MB and CR, respectively. A series of characterizations showed that the SGGO triple-network composite aerogel is a promising candidate for dye wastewater treatment.

Acknowledgements This work was supported by the National Natural Science Foundation of China (NSFC) (Grant No. 51803004), Talent Project of Anhui Agricultural University (yj2018-18) and University Natural Science Research Project of Anhui Province (KJ2016A236).

Compliance with Ethical Standard

Conflict of interest The authors declare that they have no conflict of interest.

References

1. Dai L, Zhu W, He L, Tan F, Zhu N, Zhou Q, He M, Hu G (2018) Calcium-rich biochar from crab shell: an unexpected super adsorbent for dye removal. Bioresour Technol 267:510–516
2. Song W, Gao B, Xu X, Xing L, Han S, Duan P, Song W, Jia R (2016) Adsorption–desorption behavior of magnetic amine/Fe_3O_4 functionalized biopolymer resin towards anionic dyes from wastewater. Bioresour Technol 210:123–130
3. Aroguz AZ, Gulen J, Evers R (2008) Adsorption of methylene blue from aqueous solution on pyrolyzed petrified sediment. Bioresour Technol 99(6):1503–1508
4. Huang H, Liu J, Zhang P, Zhang D, Gao F (2017) Investigation on the simultaneous removal of fluoride, ammonia nitrogen and phosphate from semiconductor wastewater using chemical precipitation. Chem Eng J 307:696–706
5. El Samrani AG, Lartiges BS, Villieras F (2008) Chemical coagulation of combined sewer overflow: heavy metal removal and treatment optimization. Water Res 42(4–5):951–960
6. Wang L (2009) Aqueous organic dye discoloration induced by contact glow discharge electrolysis. J Hazard Mater 171(1–3):577–581
7. Yang Y, Zhao B, Tang P, Cao Z, Huang M, Tan S (2014) Flexible counter electrodes based on nitrogen-doped carbon aerogels with tunable pore structure for high-performance dye-sensitized solar cells. Carbon 77:113–121
8. Mohammed N, Grishkewich N, Berry RM, Tam KC (2015) Cellulose nanocrystal–alginate hydrogel beads as novel adsorbents for organic dyes in aqueous solutions. Cellulose 22(6):3725–3738
9. Barquist K, Larsen SC (2010) Chromate adsorption on bifunctional, magnetic zeolite composites. Micropor Mesopor Mat 130(1–3):197–202
10. Gesser H, Goswami P (1989) Aerogels and related porous materials. Chem Rev 89(4):765–788
11. Hüsing N, Schubert U (1998) Aerogels—airy materials: chemistry, structure, and properties. Angew Chem Int Ed 37(1–2):22–45
12. Jiao C, Xiong J, Tao J, Xu S, Zhang D, Lin H, Chen Y (2016) Sodium alginate/graphene oxide aerogel with enhanced strength-toughness and its heavy metal adsorption study. Int J Biol Macromol 83:133–141
13. Wang L, Shelton RM, Cooper PR, Lawson M, Triffitt JT, Barralet JE (2003) Evaluation of sodium alginate for bone marrow cell tissue engineering. Biomaterials 24(20):3475–3481
14. Rocher V, Siaugue J-M, Cabuil V, Bee A (2008) Removal of organic dyes by magnetic alginate beads. Water Res 42(4–5):1290–1298
15. Pettignano A, Tanchoux N, Cacciaguerra T, Vincent T, Bernardi L, Guibal E, Quignard F (2017) Sodium and acidic alginate foams with hierarchical porosity: preparation, characterization and efficiency as a dye adsorbent. Carbohyd Polym 178:78–85
16. Deze EG, Papageorgiou SK, Favvas EP, Katsaros FK (2012) Porous alginate aerogel beads for effective and rapid heavy metal sorption from aqueous solutions: effect of porosity in Cu^{2+} and Cd^{2+} ion sorption. Chem Eng J 209:537–546
17. Wan Y, Chen X, Xiong G, Guo R, Luo H (2014) Synthesis and characterization of three-dimensional porous graphene oxide/sodium alginate scaffolds with enhanced mechanical properties. Materials Express 4(5):429–434
18. Liu S, Li Y, Li L (2017) Enhanced stability and mechanical strength of sodium alginate composite films. Carbohyd Polym 160:62–70
19. Zhu T, Teng K, Shi J, Chen L, Xu Z (2016) A facile assembly of 3D robust double network graphene/polyacrylamide architectures via γ-ray irradiation. Compos Sci Technol 123:276–285
20. Zu G, Kanamori K, Shimizu T, Zhu Y, Maeno A, Kaji H, Nakanishi K, Shen J (2018) Versatile double-cross-linking approach to transparent, machinable, supercompressible, highly bendable aerogel thermal superinsulators. Chem Mater 30(8):2759–2770
21. Bao Z, Xian C, Yuan Q, Liu G, Wu J (2019) natural polymer-based hydrogels with enhanced mechanical performances: preparation, structure, and property. Adv Healthc Mater 8(17):1900670
22. Liu G, Yuan Q, Hollett G, Zhao W, Kang Y, Wu J (2018) Cyclodextrin-based host–guest supramolecular hydrogel and its application in biomedical fields. Polym Chem 9(25):3436–3449
23. May M, Wang H, Akid R (2010) Effects of the addition of inorganic nanoparticles on the adhesive strength of a hybrid sol–gel epoxy system. Int J Adhes 30(6):505–512
24. Wang C, Xiong Y, Fan B, Yao Q, Wang H, Jin C, Sun Q (2016) Cellulose as an adhesion agent for the synthesis of lignin aerogel with strong mechanical performance. Sound-absorption Therm Insulation Sci Rep 6:32383
25. Lin N, Meng Z, Toh GW, Zhen Y, Diao Y, Xu H, Liu XY (2015) Engineering of fluorescent emission of silk fibroin composite materials by material assembly. Small 11(9–10):1205–1214
26. Tabata Y, Ikada Y (1998) Protein release from gelatin matrices. Adv Drug Deliver Rev 31(3):287–301
27. Liu C, Liu H, Xu A, Tang K, Huang Y, Lu C (2017) In situ reduced and assembled three-dimensional graphene aerogel for efficient dye removal. J Alloy Compound 714:522–529
28. Jiang J, Zhang Q, Zhan X, Chen F (2019) A multifunctional gelatin-based aerogel with superior pollutants adsorption, oil/water separation and photocatalytic properties. Chem Eng J 358:1539–1551

29. Devi N, Kakati DK (2013) Smart porous microparticles based on gelatin/sodium alginate polyelectrolyte complex. J Food Eng 117(2):193–204
30. He Y, Zhang N, Gong Q, Qiu H, Wang W, Liu Y, Gao J (2012) Alginate/graphene oxide fibers with enhanced mechanical strength prepared by wet spinning. Carbohyd Polym 88(3):1100–1108
31. Marrella A, Lagazzo A, Barberis F, Catelani T, Quarto R, Scaglione S (2017) Enhanced mechanical performances and bioactivity of cell laden-graphene oxide/alginate hydrogels open new scenario for articular tissue engineering applications. Carbon 115:608–616
32. Fan L, Ge H, Zou S, Xiao Y, Wen H, Li Y, Feng H, Nie M (2016) Sodium alginate conjugated graphene oxide as a new carrier for drug delivery system. Int J Biol Macromol 93:582–590
33. Yun Y, Wu H, Gao J, Dai W, Deng L, Lv O, Kong Y (2020) Facile synthesis of Ca^{2+}-crosslinked sodium alginate/graphene oxide hybrids as electro- and pH-responsive drug carrier. Mat Sci Eng 108:110380
34. Valentini L, Rescignano N, Puglia D, Cardinali M (2015) Kenny J (2015) Preparation of alginate/graphene oxide hybrid films and their integration in triboelectric generators. Eur J Inorg Chem 7:1192–1197
35. Feng J, Ding H, Yang G, Wang R, Li S, Liao J, Li Z, Chen D (2017) Preparation of black-pearl reduced graphene oxide-sodium alginate hydrogel microspheres for adsorbing organic pollutants. J Colloid Interf Sci 508:387–395
36. Ma J, Jiang Z, Cao J, Yu F (2019) Enhanced adsorption for the removal of antibiotics by carbon nanotubes/graphene oxide/sodium alginate triple-network nanocomposite hydrogels in aqueous solutions. Chemosphere 242:125188
37. Mohammadi A, Doctorsafaei AH, Zia KM (2018) Alginate/calix[4]arenes modified graphene oxide nanocomposite beads: preparation, characterization, and dye adsorption studies. Int J Biol Macromol 120:1353–1361
38. Hummers WS Jr, Offeman RE (1958) Preparation of graphitic oxide. J Am Chem Soc 80(6):1339–1339
39. Ingar DK, Kjetill Ø, Olav S (1989) Alginate-based solid media for plant tissue culture. Appl Microbiol Biot 31:79–83
40. Shan S, Tang H, Zhao Y, Wang W, Cui F (2019) Highly porous zirconium-crosslinked graphene oxide/alginate aerogel beads for enhanced phosphate removal. Chem Eng J 359:779–789
41. Lawrie G, Keen I, Drew B, Chandler-Temple A, Rintoul L, Fredericks P, Grøndahl L (2007) Interactions between alginate and chitosan biopolymers characterized using FTIR and XPS. Biomacromol 8(8):2533–2541
42. Yang C, Xu L, Zhou Y, Zhang X, Huang X, Wang M, Han Y, Zhai M, Wei S, Li J (2010) A green fabrication approach of gelatin/CM-chitosan hybrid hydrogel for wound healing. Carbohyd Polym 82(4):1297–1305
43. Liu L, Li C, Bao C, Jia Q, Xiao P, Liu X, Zhang Q (2012) Preparation and characterization of chitosan/graphene oxide composites for the adsorption of Au(III) and Pd(II). Talanta 93:350–357
44. Kim KH, Oh Y, Islam M (2012) Graphene coating makes carbon nanotube aerogels superelastic and resistant to fatigue. Nat Nanotechnol 7(9):562
45. Liu C, Liu H, Xiong T, Xu A, Pan B, Tang K (2018) Graphene oxide reinforced alginate/PVA double network hydrogels for efficient dye removal. Polymers (Basel) 10(8):835
46. Piao Y, Chen B (2017) Synthesis and mechanical properties of double cross-linked gelatin-graphene oxide hydrogels. Int J Biol Macromol 101:791–798
47. Shan C, Wang L, Li Z, Zhong X, Hou Y, Zhang L, Shi F (2019) Graphene oxide enhanced polyacrylamide-alginate aerogels catalysts. Carbohydr Polym 203:19–25
48. Liu L, Gao ZY, Su XP, Chen X, Jiang L, Yao JM (2015) Adsorption removal of dyes from single and binary solutions using a cellulose-based bioadsorbent. ACS Sustain Chem Eng 3(3):432–442
49. Aldegs Y, Elbarghouthi M, Elsheikh A, Walker G (2008) Effect of solution pH, ionic strength, and temperature on adsorption behavior of reactive dyes on activated carbon. Dyes Pigm 77(1):16–23
50. Tiwari JN, Mahesh K, Le NH, Kemp KC, Timilsina R, Tiwari RN, Kim KS (2013) Reduced graphene oxide-based hydrogels for the efficient capture of dye pollutants from aqueous solutions. Carbon 56:173–182
51. Huang X, Liao X, Shi B (2009) Hg (II) removal from aqueous solution by bayberry tannin-immobilized collagen fiber. J Hazard Mater 170(2–3):1141–1148
52. Jiao C, Tao J, Xiong J, Wang X, Zhang D, Lin H, Chen Y (2017) In situ synthesis of MnO_2-loaded biocomposite based on microcrystalline cellulose for Pb^{2+} removal from wastewater. Cellulose 24(6):2591–2604
53. Tao J, Xiong J, Jiao C, Zhang D, Lin H, Chen Y (2016) Hybrid Mesoporous Silica Based on Hyperbranch-Substrate Nanonetwork as Highly Efficient Adsorbent for Water Treatment. ACS Sustain Chem Eng 4(1):60–68
54. Langmuir I (1918) The adsorption of gases on plane surfaces of glass, mica and platinum. J Am Chem Soc 40(9):1361–1403
55. Xu J, Wang L, Zhu Y (2012) Decontamination of bisphenol A from aqueous solution by graphene adsorption. Langmuir 28(22):8418–8425
56. Kumar KV, Kumaran A (2005) Removal of methylene blue by mango seed kernel powder. Biochem Eng J 27(1):83–93
57. Nollet H, Roels M, Lutgen P, Van der Meeren P, Verstraete W (2003) Removal of PCBs from wastewater using fly ash. Chemosphere 53(6):655–665
58. Kuo CY, Wu CH, Wu JY (2008) Adsorption of direct dyes from aqueous solutions by carbon nanotubes: determination of equilibrium, kinetics and thermodynamics parameters. J Colloid Interface Sci 327(2):308–315